ISSN 0031-918X, Physics of Metals and Metallography, 2022, Vol. 123, No. 14, pp. 1419–1426. © Pleiades Publishing, Ltd., 2022.
ISSN 0031-918X, Physics of Metals and Metallography, 2022. © Pleiades Publishing, Ltd., 2022.

STRUCTURE, PHASE TRANSFORMATIONS, AND DIFFUSION

Microstructure, Wear and Corrosion Resistance of $AlNi_2Ti$–Ti_2Ni–NiTi Intermetallic Alloy

H. X. Zhang*

Department of Mechanical Manufacturing, Xinxiang Vocational and Technical College, Xinxiang 453006 China

**e-mail: zhang168134@163.com*

Received December 15, 2021; revised April 8, 2022; accepted April 14, 2022

Abstract—$AlNi_2Ti$–Ti_2Ni–NiTi intermetallic alloy consisting of $AlNi_2Ti$ primary dendrites and Ti_2Ni–NiTi interdendritic phase was fabricated by vacuum arc melting process. Corrosion and wear behaviors of the alloy were characterized using potentiodynamic polarization, electrochemical impedance spectroscopy (EIS) and wear tests. Electrochemical measurements indicated that the alloy exhibited an excellent corrosion resistance in 0.5 mol/L H_2SO_4 solutions with a high corrosion potential and wide passivation region (0–1.2 V) due to the formation of compact and protective passive films (TiO_2 and Al_2O_3). Due to the high hardness and strong covalent bonding $AlNi_2Ti$–Ti_2Ni–NiTi alloys exhibit excellent wear resistance with a low friction coefficient and wear rate under dry sliding wear conditions. The dominant wear mechanisms of the alloy are friction stress-induced micro-fracture and tribo-oxidation.

Keywords: $AlNi_2Ti$–Ti_2Ni–NiTi, electrochemical corrosion, arc melting, wear resistance

DOI: 10.1134/S0031918X21101142

INTRODUCTION

With the development of aerospace technology, the traditional Ni-based alloy has reached the upper limit of use [1, 2]. It is urgent to develop a new type of high temperature structural materials with excellent comprehensive properties such as low density and high strength, excellent corrosion resistance and wear resistance. In the Al–Ni–Ti ternary system, several binary and ternary intermetallic compounds with attractive physical and mechanical properties have been subjected to increased interest in recent years [3]. Among those compounds, nickel-titanium compounds such as isoatomic component NiTi exhibit a good intrinsic plasticity and shape memory behavior [4, 5]. Ti_2Ni and Ni_3Ti intermetallic compounds offer more attractive properties for high temperature structural applications [6]. However, like other intermetallic compounds, high room temperature brittleness and insufficient creep resistance at high temperature are the main obstacles to its practical application [7].

Ternary intermetallic compounds generally exhibited better toughness than binary intermetallics under the conditions of maintaining their high hardness and strong interatomic binding [8]. Up to now, there are four ternary intermetallics identified as $Al_{13}Ni_2Ti_5$ ($\tau1$), Al_2NiTi ($\tau2$), Al_3NiTi_2 ($\tau3$) and $AlNi_2Ti$ ($\tau4$) in the Al–Ni–Ti system by thermodynamic calculation and experimental observation [9–11]. Among these compounds, $L2_1$(Heusler alloy)-$AlNi_2Ti$ compound has a high melting point (1503°C), strength and hardness, and has been extensively studied as a strengthening phase of nickel-based, iron-based superalloy [12, 13]. It is found that the strengthening phase $AlNi_2Ti$ and the matrix NiTi can form a coherent interface $AlNi_2Ti$/NiTi multiphase structure, and its room temperature compression strength is as high as 2300 MPa [14]. Therefore, NiTi/$AlNi_2Ti$ based materials are expected to have good comprehensive mechanical properties (high strength and toughness), which is similar to the traditional γ/γ' structure of nickel-based superalloys [15]. At the same time, the $AlNi_2Ti$ ternary intermetallic compound has high passivation components (Al and Ti elements) and strong covalent bonding characteristics, which make it desirable to have excellent corrosion and wear resistance. Therefore, $AlNi_2Ti$-based alloy is anticipated to be a novel wear and corrosion resistant material under harsh conditions. However, to the best of our knowledge, there is no study on the wear and corrosion behavior of $AlNi_2Ti$ Heusler alloy. In this present paper, a novel wear and corrosion resistant $AlNi_2Ti$–Ti_2Ni–NiTi intermetallic alloy was developed and prepared by vacuum arc melting. The electrochemical corrosion and wear resistance was investigated.

EXPERIMENTAL

Pure aluminum (99.8%), nickel (99.9%) and titanium (99.9%) elemental powders with an average particle size ranging from 40 to 100 μm were selected as

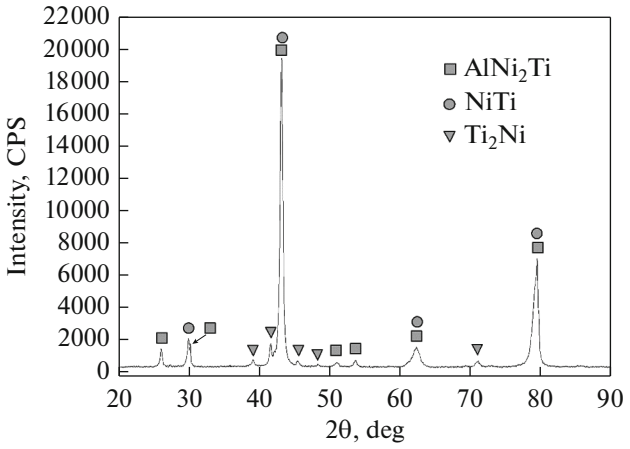

Fig. 1. XRD pattern of the $AlNi_2Ti$–Ti_2Ni–NiTi alloy.

raw materials. $AlNi_2Ti$–Ti_2Ni–NiTi alloy was synthesized by arc melting stoichiometric composition (at %) of 12.6Al–43Ni–45.4Ti in a water-cooled copper crucible arc melting furnace with an electromagnetic stirring device under an argon atmosphere. Each ingot was re-melted five times and the ingot was flipped before each re-melting to ensure the homogeneity of the alloy composition. The cast ingots were cut into 10 × 10 × 5 mm specimens using electro-discharge machining (EDM) for microstructure, corrosion and wear tests.

The phase composition of the samples was investigated by means of X-ray diffraction (XRD, D/Dmax-2400, Rigaku, Japan) with Cu$K\alpha$ radiation (λ = 0.15418 nm). Prior to microstructural analysis, the samples were mechanically polished and then chemically etched with saturated $FeCl_3$ and HCl solutions for 10–15 s. Microstructure of the alloy ingots was characterized by field-emission scanning electron microscopy (FESEM, JSM-6700F, JEOL, Japan) equipped with an energy dispersive spectroscopy (EDS). The hardness of the alloys was measured using a Vickers micro hardness tester (HVS-1000, Yantai Huayin testing instrument Co., Ltd., China) with a load of 9.8 N for 10 s. The values of hardness were the average of five tests.

The corrosion behaviors of the alloys were investigated in 0.5 mol/L H_2SO_4 solutions using electrochemical test equipment (PGSTAT302N, Switzerland). Electrochemical tests adopt a three-electrode system, in which the high purity platinum sheet was used as the counter electrode, the alloy samples were used as the working electrode, and a saturated calomel electrode (SCE) was used as the reference electrode. The potentiodynamic anodic polarization curves were recorded from a steady open-circuit potential with a scanning speed of 2 mV/s. EIS measurement was performed at an open-circuit potential with a 5 mV amplitude signal and applied frequency ranged from 10^5 to 10^{-2} Hz.

The dry sliding wear behaviors of the alloys were carried out using a ball-on-flat reciprocating sliding tribometer (MFT-4000, Lanzhou Institute of Chemical Physics, Chinese Academy of Sciences, Lanzhou, China) at room temperature. $AlNi_2Ti$–Ti_2Ni–NiTi specimens were sliding against a 6 mm diameter ball made of GCr15 bearing steel for dry sliding wear testing. The dry sliding wear tests were performed at 2, 5, 10 N loads, and the amplitude length was 5 mm, the vibration frequency was 5 Hz, and the sliding time was 30 min. Commercial traditional austenitic stainless steel 1Cr18Ni9Ti was selected as a reference material for electrochemical corrosion and dry sliding wear tests. The corrosion and wear morphologies with corresponding compositional analyses were investigated by SEM and EDS, respectively.

RESULTS AND DISCUSSION

3.1. Microstructure

X-ray diffraction pattern of arc-melted $AlNi_2Ti$–Ti_2Ni–NiTi alloy is shown in Fig. 1. It can be seen that the main constituents of the alloy are $AlNi_2Ti$, NiTi and a small amount of Ti_2Ni. As shown in Fig. 2, the alloy has a uniform and compact microstructure and no obvious defects such as pores and microcracks, which is mainly composed of primary dendrites and interdendritic phase. Results of the EDS analysis shows that the average chemical composition (at %) of the primary dendrites and interdendritic phases is 26.08Al–50.46Ni–23.46Ti and 7.72Al–42.32Ni–50.06Ti, respectively. Combined with the results of XRD and EDS analysis, the primary dendrite is identified as the $AlNi_2Ti$ intermetallic phase and the interdendritic phase is a mixture of NiTi–Ti_2Ni phases.

In the Al–Ni–Ti ternary alloy system, the $AlNi_2Ti$ intermetallic compound has a higher melting point, and firstly precipitates from the liquid phase to form a primary dendritic phase during arc melted [16]. With the precipitation of $AlNi_2Ti$ phase, Ni and Ti elements are gradually enriched in residual liquids and transformed into Ti_2Ni–NiTi phase. The volume fraction of the primary dendrite of $AlNi_2Ti$ is determined to be about 89% according to the SEM morphology of Fig. 2. The average hardness of the $AlNi_2Ti$–Ti_2Ni–NiTi alloy was found to be approximately 792 ± 36 HV due to the high volume fraction of the high hardness $AlNi_2Ti$ intermetallic compound.

3.2. Electrochemical Corrosion Behaviors

The potentio-dynamic anodic polarization curves of $AlNi_2Ti$–Ti_2Ni–NiTi alloy and austenitic stainless steel 1Cr18Ni9Ti in 0.5 mol/L H_2SO_4 solutions open to air are shown in Fig. 3. The anodic polarization

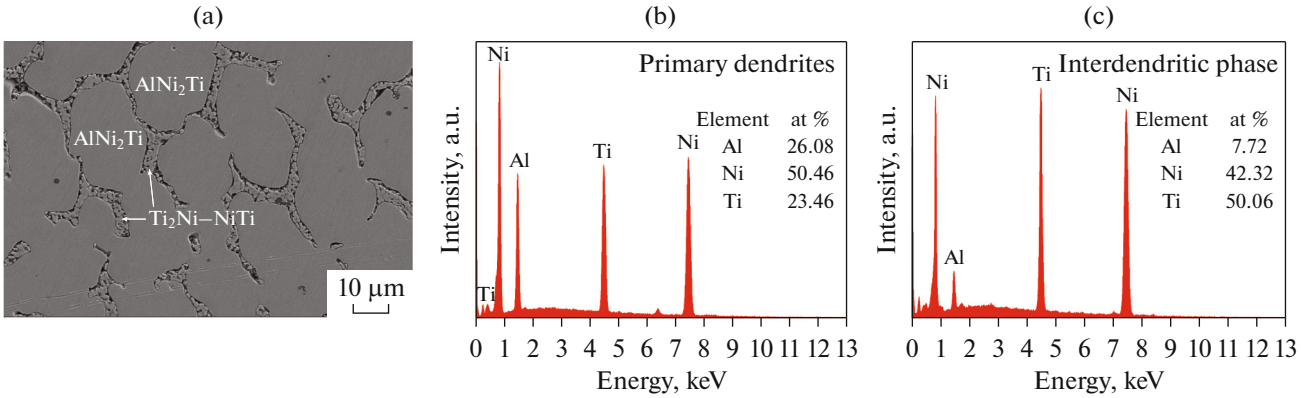

Fig. 2. Microstructure (a) and EDS spectra (b and c) of $AlNi_2Ti–Ti_2Ni–NiTi$ alloy.

curves of the alloy and 1Cr18Ni9Ti material in H_2SO_4 solution show no significant difference in shape. However, the breakdown potential of $AlNi_2Ti–Ti_2Ni–NiTi$ alloy (up to 1200 mV) is 400 mV higher than austenitic stainless steel 1Cr18Ni9Ti (about 800 mV). Moreover, the alloy exhibits a high corrosion potential and a wide passivation region range from 0 to 1.2 V compared to austenitic stainless steel 1Cr18Ni9Ti, which suggested that $NiTi/AlNi_2Ti$ alloy has an excellent corrosion resistance in 0.5mol/L H_2SO_4 solution.

The representative Nyquist and Bode plots of $AlNi_2Ti–Ti_2Ni–NiTi$ alloy and the reference material 1Cr18Ni9Ti measured at their open circuit potentials in 0.5 mol/L H_2SO_4 solution at room temperature were presented in Figs. 4a, 4b, respectively. It is worth noting that the curves of the test samples are different in shape, indicating that they follow different corrosion mechanisms. From Fig. 4, semicircles and one time-constant are observed in the Nyquist and Bode plots of the reference material 1Cr18Ni9Ti. In contrast, the Nyquist and Bode plots of the $AlNi_2Ti–Ti_2Ni–NiTi$ alloy exhibit an incomplete semicircle and two time-constants, suggesting that an additional reaction might have occurred at the boundaries between the primary dendritic $AlNi_2Ti$ and the interdendritic phase. Therefore, the equivalent circuit models in Figs. 5a, 5b can be used to fit the electrochemical reactions of $AlNi_2Ti–Ti_2Ni–NiTi$ alloy and reference material 1Cr18Ni9Ti in 0.5 mol/L H_2SO_4 solution, respectively.

Some empirical equivalent circuit models are used to fit the experimental impedance data of passivated materials (for example, pure metals, alloys and some intermetallic compounds) [17]. Among these models, $R_s(Q_1R_{ct})$ and $R_s(Q_1(R_p(Q_2R_{ct})))$ are the most widely used. $R_s(Q_1R_{ct})$ model suggests that a single compact passive film is formed instantaneously on the electrode surface [18]. In the two equivalent circuit models, R_s represents the solution impedance and R_p is the passive film impedance. R_{ct} represents the interface charge transfer impedance, which reflects the corrosion rate of the material. In general, the larger the R_{ct}, the slower the corrosion rate of the material [19]. CPE ($Q1$ and $Q2$) are represents the constant phase element. Its impedance is given by Eq. (1):

$$Z_{CPE} = \left(\frac{1}{Y_0}\right)\left[(j\omega)^n\right]^{-1}, \quad (1)$$

where Y_0 is equal to the capacitance, j is the complex operator, ω is the angular frequency, n is an empirical exponent, which describes the deviation of the electrochemical reaction from the ideal RC-behavior due to surface inhomogeneities, roughness effects and variations in the properties or compositions of surface layers [20]. The values of n are usually related to the roughness of the electrode surface, and a low value of n can be attributed to the roughening of the electrode surface due to erosion in corrosion studies [21]. Table 1 shows the fitted electrochemical parameters according

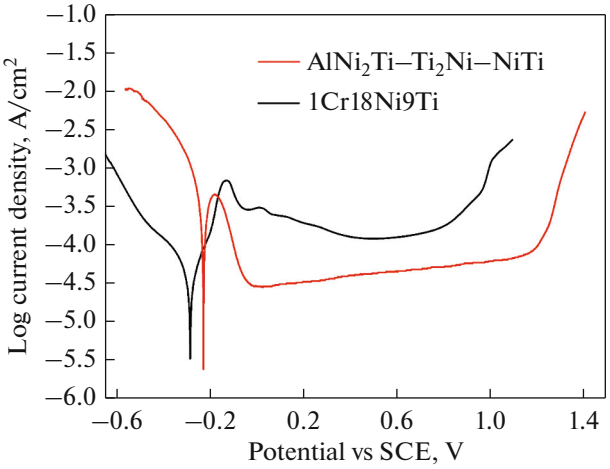

Fig. 3. Anodic polarization curves of the $AlNi_2Ti–Ti_2Ni–NiTi$ alloy and the reference material 1Cr18Ni9Ti in 0.5 mol/L H_2SO_4 water solutions.

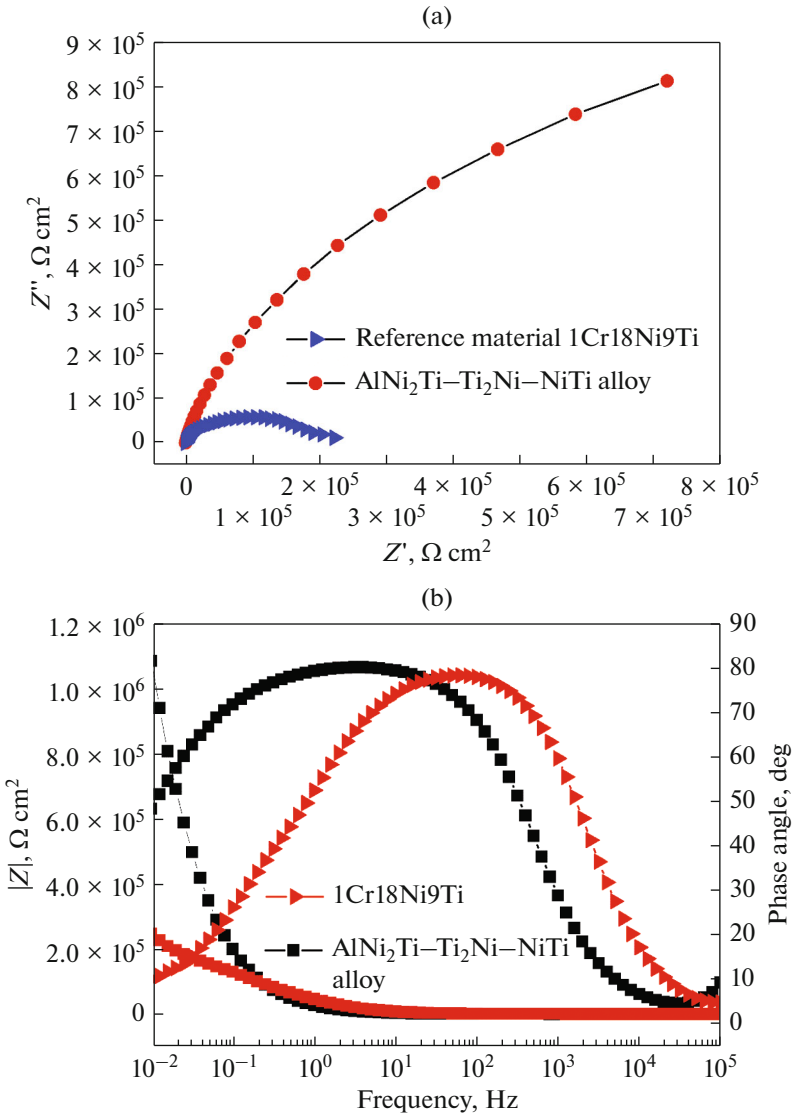

Fig. 4. Nyquist (a) and Bode (b) plots of the $AlNi_2Ti–Ti_2Ni–NiTi$ alloy and the reference material 1Cr18Ni9Ti in 0.5 mol/L H_2SO_4 solution.

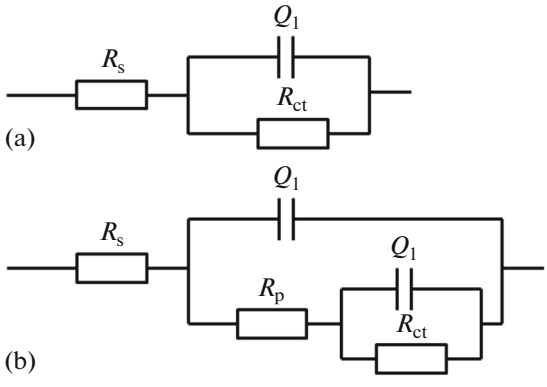

Fig. 5. Equivalent electrical circuit model used to fit the experimental impedance data. (a) 1Cr18Ni9Ti and (b) $AlNi_2Ti–Ti_2Ni–NiTi$ alloy.

to the EIS results using the equivalent circuit model in Fig. 5. Comparatively, the R_{ct} of $AlNi_2Ti–Ti_2Ni–NiTi$ alloy was nearly six times higher than that of reference material 1Cr18Ni9Ti, which indicates that $AlNi_2Ti–Ti_2Ni–NiTi$ alloy has superior corrosion resistance to 1Cr18Ni9Ti in 0.5 mol/L H_2SO_4 solution.

It is generally believed that the corrosion behavior of the alloy mainly depends on its composition, chemical stability and corrosion environment [22]. For the $AlNi_2Ti–Ti_2Ni–NiTi$ alloy, Ti, Ni and Al are all strong passive elements, especially the Ti and Al component element, a stable and compact TiO_2 and Al_2O_3 passive film is easily formed in acidic and neutral solutions [23, 24]. The $AlNi_2Ti–Ti_2Ni–NiTi$ alloy containing a large amount of Ti and Al element to exhibit an excellent corrosion resistance in 0.5 mol/L H_2SO_4

Table 1. Impedance fitting parameters of $AlNi_2Ti–Ti_2Ni–NiTi$ alloy and 1Cr18Ni9Ti in 0.5 mol/L H_2SO_4 solution

Samples	R_s, Ω	R_p, Ω cm^2	Q_1, μF cm^{-2}	n_1	Q_2, μF cm^{-2}	n_2	R_{ct}, Ω cm^2
1Cr18Ni9Ti	12.15	/	23.1	0.89	/	/	101.2
$AlNi_2Ti–Ti_2Ni–NiTi$	6.37	13.38	0.37	0.95	34.3	0.93	595.3

solution. Furthermore, strong convection, electromagnetic agitation and rapid cooling during the arc melting can improve the structural and chemical stability of $AlNi_2Ti–Ti_2Ni–NiTi$ alloy [25]. In addition, the constituent phases of $AlNi_2Ti$ and $Ti_2Ni–NiTi$ are intermetallic compounds, and their strong atomic bonds and high chemical stability also make an important contribution to the excellent corrosion resistance of the $AlNi_2Ti–Ti_2Ni–NiTi$ alloy in 0.5 mol/L H_2SO_4 solution.

3.3. Friction and Wear Properties

The friction and wear properties of $AlNi_2Ti–Ti_2Ni–NiTi$ alloy and reference material 1Cr18Ni9Ti were studied by sliding against GCr15 bearing steel ball under different loads, as shown in Fig. 6. It is obvious that the friction coefficient curve of $AlNi_2Ti–Ti_2Ni–NiTi$ alloy could be divided into three different stages: first, the friction coefficients of the alloy increase rapidly at the initial running-in stage, and then enters a non-stable stage at the first 1 to 10 min with a large fluctuation of friction coefficients, followed by a stable stage where the coefficients of friction fluctuate within a narrow range around the average value. It is worth noting that an obvious coefficient fluctuation is observed at 2 N loads, whereas this fluctuation is minimal at 5 and 10 N loads. According to Murthy's research, the fluctuation of the friction coefficient during sliding is mainly related to the surface state of the friction contact area, which can be attributed to the presence of three body (wear debris) during sliding [26]. In addition, for the $AlNi_2Ti–Ti_2Ni–NiTi$ alloy, the friction coefficients decrease with an increasing load, whereas the friction coefficient of the reference material 1Cr18Ni9Ti increases with an increase in applied load, as shown in Fig. 7. The average friction coefficient values of $AlNi_2Ti–Ti_2Ni–NiTi$ alloy and reference material 1Cr18Ni9 are (0.462, 0.565), (0.409, 0.592) and (0.287, 0.611) at 2, 5, and 10 N, respectively. Compared with the reference material 1Cr18Ni9Ti, the average friction coefficient of $AlNi_2Ti–Ti_2Ni–NiTi$ alloy is lower under all experimental loads.

The specific wear rates of the samples are calculated by volume loss, applied load and total sliding distance according to the formula:

$$W = \frac{V}{LN}, \tag{2}$$

where $V = AS$ is the wear volume (mm^3), A is area of the cross-section (mm^2)(cross-sections of worn scars of the specimens were measured using a surface profilometer (MicroXAM) after the wear tests), and S is the length of the stroke (mm), L is the total sliding dis-

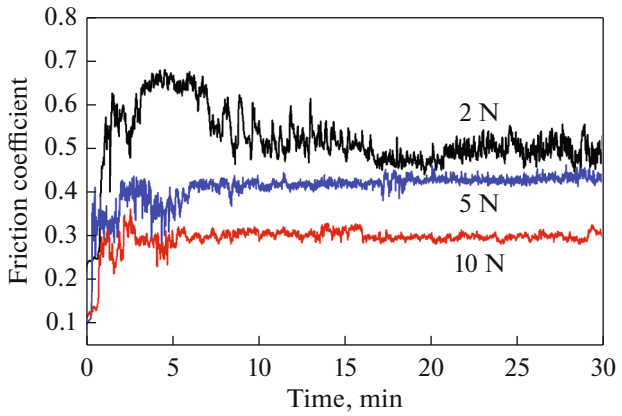

Fig. 6. Coefficient of friction vs. sliding times for $AlNi_2Ti–Ti_2Ni–NiTi$ alloy sliding against GCr15 bearing ball under the normal loads of 2, 5, and 10 N.

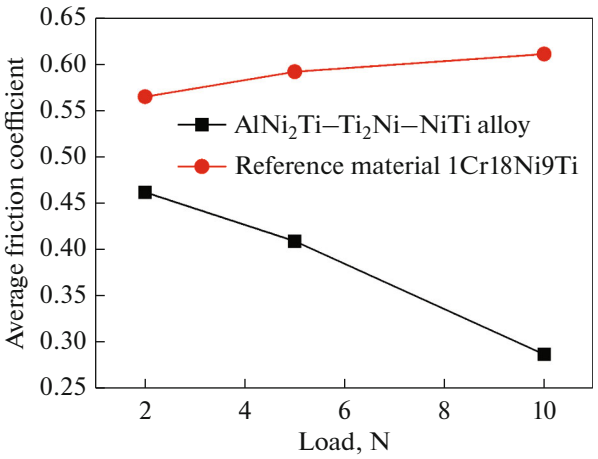

Fig. 7. Change in the average value of the friction coefficient of $AlNi_2Ti–Ti_2Ni–NiTi$ alloy and reference material 1Cr18Ni9Ti under different loads.

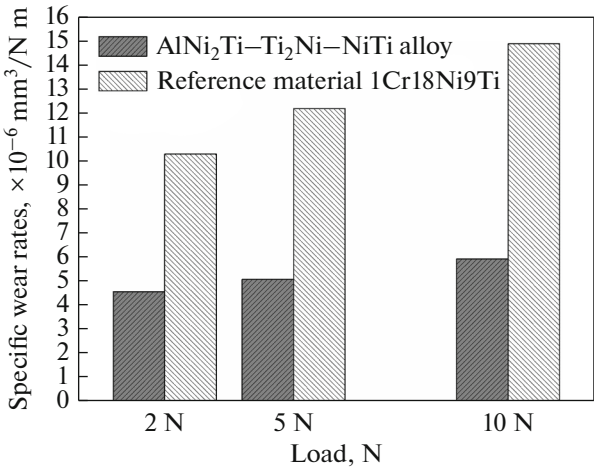

Fig. 8. Specific wear rates of the $AlNi_2Ti–Ti_2Ni–NiTi$ alloy and reference material 1Cr18Ni9Ti at different load.

tance (m), N is the experimental load (N). As shown in Fig. 8, the specific wear rates of $AlNi_2Ti–Ti_2Ni–NiTi$ alloy and reference material 1Cr18Ni9Ti increase with the increase of applied load at room temperature. In addition, compared with $AlNi_2Ti–Ti_2Ni–NiTi$ alloy, the specific wear rates of the reference material 1Cr18Ni9Ti increase obviously with the test load increases. More importantly, the specific wear rates of $AlNi_2Ti–Ti_2Ni–NiTi$ alloy are significantly lower than that of reference materials 1Cr18Ni9Ti under all loads. The specific wear rates of the $AlNi_2Ti–Ti_2Ni–NiTi$ alloy decrease by one order of magnitude. The specific wear rate values of $AlNi_2Ti–Ti_2Ni–NiTi$ alloy are 4.56×10^{-6}, 5.07×10^{-6} and 5.93×10^{-6} mm^3/N m at 2, 5 and 10 N, respectively.

Figure 9 shows the SEM micrographs of worn surface of the samples sliding against GCr15 bearing balls under normal loads of 2 and 10 N, respectively. For $AlNi_2Ti–Ti_2Ni–NiTi$ alloy, the abrasion was commonly noticed under all loads. As shown in Fig. 9a, the worn surface of $AlNi_2Ti–Ti_2Ni–NiTi$ alloy was rough and composed of flaking craters, a small amount of debris and slight abrasive grooves at 2 N loads. This is mainly attributed to the tensile stress generated by the contact of the friction surface during the friction process. Therefore, the wear mechanism of the $AlNi_2Ti–Ti_2Ni–NiTi$ alloy was dominated by the fracture process caused by friction stress at lower loads. The formation of flaking craters make the contact condition of the wear surface unstable and forms large wear debris, which also explained that the large fluctuation of friction coefficient curve was observed under 2 N load. At the higher load of 10 N, the worn surface of $AlNi_2Ti–Ti_2Ni–NiTi$ alloy was very smooth and clean except for a small amount of fine worn debris particles, as shown in Fig. 9b. According to the EDS analysis of Fig. 10, the Al, Ni, Ti, O, and Fe elements were detected on the worn surface of $AlNi_2Ti–Ti_2Ni–NiTi$ alloy under 2 and 10 N loads. The presence of O element indicates that a tribo-oxidation reaction occurred during the wear process. The presence of the Fe element peak, suggesting that the adhesion transfer occurs from the bearing steel ball due to the lower hardness of the steel ball compared to the $AlNi_2Ti–Ti_2Ni–NiTi$ alloy. In addition, it can be seen from Fig. 10 that the intensity of Fe and O element peaks increases with the increase of loads, which indicates that the high load is more beneficial to the adhesion transfer of Fe and the occurrence of friction oxidation reaction. Compared to the $AlNi_2Ti–Ti_2Ni–NiTi$ alloy, the apparent grooves, adhesion and deformation characteristics were observed on the wear surface of the reference material 1Cr18Ni9Ti, as shown in Fig. 9c.

CONCLUSIONS

Corrosion and wear properties of $AlNi_2Ti–Ti_2Ni–NiTi$ intermetallic alloy were investigated by corrosion and wear test. The following conclusions can be drawn:

(1) A novel corrosion-resistant $AlNi_2Ti–Ti_2Ni–NiTi$ intermetallic alloy was fabricated by arc melting process with a microstructure consisting of the pri-

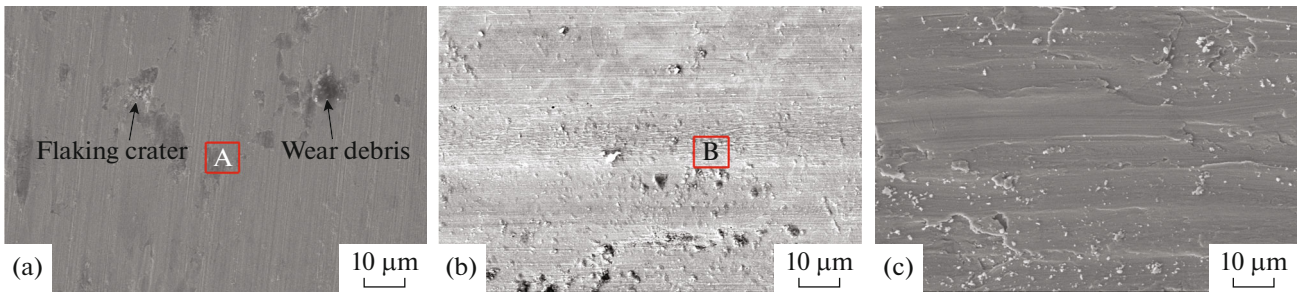

Fig. 9. SEM micrographs of worn surface of the $AlNi_2Ti–Ti_2Ni–NiTi$ alloy (a and b) and reference material 1Cr18Ni9Ti (c) sliding against GCr15 steel balls under different load. (a) 2 and (b and c) 10 N.

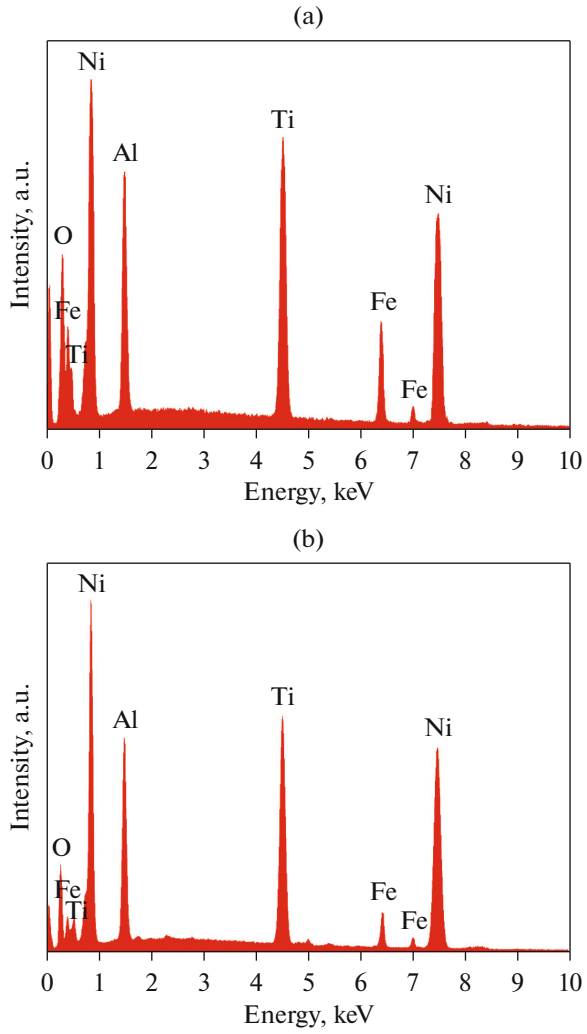

Fig. 10. EDS patterns of the marked position A in Fig. 9a and position B in Fig. 9b.

mary dendrites $AlNi_2Ti$ and interdendritic phase of Ti_2Ni–NiTi.

(2) $AlNi_2Ti$–Ti_2Ni–NiTi alloy exhibits an excellent corrosion resistance in 0.5 mol/L H_2SO_4 solution with a more positive corrosion potential and a wider passive potential range than the reference material 1Cr18Ni9Ti. The passive potential range of the alloy is about twice as broad as that of 1Cr18Ni9Ti material. The excellent corrosion resistance of the $AlNi_2Ti$–Ti_2Ni–NiTi alloy is mainly due to the instantaneous formation of a stable and compact passive film composed of TiO_2 and Al_2O_3. The structural and chemical consistency and the inherent strong inter-atomic bonding of the $AlNi_2Ti$ and Ti_2Ni–NiTi intermetallic are also important factors for the high corrosion resistance of the alloy.

(3) The $AlNi_2Ti$–Ti_2Ni–NiTi alloy has an excellent wear resistance accompanied by a low friction coefficient and wear rate under dry sliding wear conditions attributed to its high hardness (792 HV) and strong covalent dominated bonding. The main wear mechanisms of the $AlNi_2Ti$–Ti_2Ni–NiTi alloy are fracture processes induced by frictional stress at low loads and tribological oxidation at high loads.

ACKNOWLEDGMENTS

The authors acknowledge Mr. Deshun Liu for their assistance on experiments of arc melting.

FUNDING

This research was supported by the Natural Science Foundation of Shandong Province of China (Grant no. ZR2018MEM005).

CONFLICT OF INTEREST

The authors declare that they have no conflicts of interest.

REFERENCES

1. Y. H. Liu, Z. K. Yao, Y. Q. Ning, Y. Nan, H. Z. Guo, C. Qin, and Z. F. Shi, "The flow behavior and constitutive equation in isothermal compression of FGH4096-GH4133B dual alloy," Mater. Des. **63**, 829–837 (2014).
2. H. Chen, Y. T. Liu, Y. Zhao, and Z. W. Wang, "Characterization, formation mechanism, and thermodynamics of nanocrystalline Ni_3Si powder prepared by mechanical alloying," Phys. Met. Metallogr. **121**, 1266–1272 (2020).
3. G. Song, Z. Q. Sun, J. D. Poplawsky, Y. F. Gao, and P. K. Liaw, "Microstructural evolution of single Ni_2TiAl or hierarchical NiAl/Ni_2TiAl precipitates in Fe–Ni–Al–Cr–Ti ferritic alloys during thermal treatment for elevated-temperature applications," Acta Mater. **127**, 1–16 (2017).
4. K. Otsuka and X. Ren, "Physical metallurgy of Ti–Ni-based shape memory alloys," Prog. Mater. Sci. **50**, 511–678 (2005).
5. M. Mohri, M. Nili-Ahmadabadi, M. Pouryazdan-Panah, and H. Hahn, "Evaluation of structure and mechanical properties of Ni-rich NiTi/Kapton composite film," Mater. Sci. Eng., A **668**, 13–9 (2016).
6. M. H. Elahinia, M. Hashemi, M. Tabesh, and S. B. Bhaduri, "Manufacturing and processing of NiTi implants: a review," Prog. Mater. Sci. **57**, 911–946 (2012).
7. H. Chen, D. M. Zhou, L. Cai, Y. Y. Wang, and K. Yu, "Characterization and formation mechanism of Ni_3Si–Al_2O_3 nanocomposite prepared by mechanochemical reduction method," Metall. Mater. Int. **26**, 230–239 (2020).
8. L. Yuan and H. M. Wang, "Corrosion properties of a $Cr_{13}Ni_5Si_2$-based metal silicide alloy," Intermetallics **16**, 1149–1155 (2008).
9. A. Dębski, W.Gąsior, A. Sypień, and A. Góral, "Enthalpy of formation of intermetallic phases from Al–Ni

and Al–Ni–Ti systems," Intermetallics **42**, 92–98 (2013).

10. J. C. Schuster, Z. Pan, S. H. Liu, F. Weitzer, and Y. Du, "On the constitution of ternary system Al–Ni–Ti," Intermetallics **15**, 1257–1267 (2007).
11. V. Raghavan, "Al–Ni–Ti (aluminum-nickel-titanium)," J. Phase Equilib. Diffus. **31**, 55–56 (2010).
12. G. Song, Z. Q. Sun, B. Clausen, and P. K. Liaw, "Microstructural characteristics of a Ni_2TiAl–precipitate-strengthened ferritic alloy," J. Alloys Compd. **693**, 921–928 (2017).
13. C. H. Liebscher, V. R. Radmilović, U. Dahmen, N. Q. Vo, D. C. Dunand, M. Asta, and G. Ghosh, "A hierarchical microstructure due to chemical ordering in the bcc lattice: Early stages of formation in a ferritic Fe–Al–Cr–Ni–Ti alloy," Acta Mater. **92**, 220–232 (2015).
14. Y. Koizumi, Y. Ro, S. Nakazawa, and H. Harada, "NiTi-base intermetallic alioys strengthened by Al substitution," Mater. Sci. Eng., A **223**, 36–41 (1997).
15. P. Warren, Y. Murakami, and H. Harada, "Phase separation in NiTi–Ni_2TiAl alloy system," Mater. Sci. Eng., A **223**, 17–20 (1997).
16. H. Chen, Z. Zhang, X. H. Hao, B. X. Huang, X. C. Zhao, and C. C. Hu, "Microstructure and tribocorrosion properties of NiTi/$AlNi_2Ti$ ternary intermetallic alloy," Vacuum **184**, 109928 (2021).
17. J. Xu, L. L. Liu, P. Munroe, Z. H. Xie, and Z. T. Jiang, "The nature and role of passive films in controlling the corrosion resistance of $MoSi_2$-based nanocomposite coatings," J. Mater. Chem. A **1**, 10281–10291 (2013).
18. V. D. Jovic and M. W. Barsoum, "Corrosion behavior and passive film characteristics formed on Ti, Ti_3SiC_2, and Ti_4AlN_3 in H_2SO_4 and HCl," J. Electrochem. Soc. **151**, B71–B76 (2004).
19. A. B. Oliveira, A. C. Bastos, C. M. Fernandes, C. M. S. Pinho, A. M. R. Senos, E. Soares, J. Sacramento, M. L. Zheludkevich, and M. G. S. Ferreira, "Corrosion behaviour of WC–10% AISI 304 cemented carbides," Corros. Sci. **100**, 322–331 (2015).
20. J. Xu, C. H. Zhou, and S. Y. Jiang, "Investigation on corrosion behavior of sputter-deposited nanocrystalline $(Mo_xCr_{1-x})_5Si_3$ films by double cathode glow plasma," Intermetallics **18**, 1669–1675 (2010).
21. A. C. Bastos, M. G. Ferreira, and A. M. Simões, "Corrosion inhibition by chromate and phosphate extracts for iron substrates studied by EIS and SVET," Corros. Sci. **48**, 1500–1512 (2006).
22. D. Z. Wang, P. Li, K. Kang, C. Zhang, J. Yin, M. Jiang, Q. W. Hu, and X. Y. Zeng, "Corrosion behaviors of $Cr_{13}Ni_5Si_2$ based composite coatings prepared by laser-induction hybrid cladding," Surf. Coat. Technol. **300**, 128–134 (2016).
23. F. T. Cheng, P. Shi, G. K. H. Pang, M. H. Wong, and H. C. Man, "Microstructural characterization of oxide film formed on NiTi by anodization in acetic acid," J. Alloys Compd. **438**, 238–242 (2007).
24. Y. Z. Huang and D. J. Blackwood, "Characterisation of titanium oxide film grown in 0.9% NaCl at different sweep rates," Electrochim. Acta **51**, 1099–1107 (2005).
25. L. X. Dong and H. M. Wang, "Corrosion behavior of Ti_2Ni_3Si/NiTi intermetallic alloys in H_2SO_4 solution," Rare Met. Mater. Eng. **38**, 1010–1014 (2009).
26. T. S. R. Ch. Murthy, P. K. Limaye, J. K. Sonber, K. Sairam, A. Nagaraj, C. Subramanian, N. L. Soni, R. J. Patel, and R. C. Hubli, "Friction and wear properties of hot pressed $(Ti,Cr)B_2$ + $MoSi_2$ composite in sliding against WC ball," Int. J. Refract. Met. **43**, 276–283 (2014).